Theoretical analysis for AlGaN avalanche photodiodes with mesa and field plate structure*

Ke-Xiu Dong(董可秀)[1], Dun-Jun Chen(陈敦军)[2,†], Qing Cai(蔡青)[2], Yan-Li liu(刘燕丽)[3], and Yu-Jie Wang(王玉杰)[1]

[1] School of Mechanical and Electrical Engineering, Chuzhou University, Chuzhou 239000, China
[2] Key Laboratory of Advanced Photonic and Electronic Materials, School of Electronic Science and Engineering, Nanjing University, Nanjing 210093, China
[3] School of Information and Electronic Engineering, Shandong Technology and Business University, Yantai 264005, China

(Received 1 March 2020; revised manuscript received 19 April 2020; accepted manuscript online 7 May 2020)

To suppress the electric field crowding at sidewall and improve the detection sensitivity of the AlGaN separate absorption and multiplication (SAM) avalanche photodiodes (APDs), we propose the new AlGaN APDs structure combining a large-area mesa with a field plate (FP). The simulated results show that the proposed AlGaN APDs exhibit a significant increase in avalanche gain, about two orders of magnitude, compared to their counterparts without FP structure, which is attributed to the suppression of electric field crowding at sidewall of multiplication layer and the reduction of the maximum electric field at the p-type GaN sidewall in p–n depletion region. Meanwhile, the APDs can produce an obviously enhanced photocurrent due to the increase in cross sectional area of multiplication region.

Keywords: AlGaN, avalanche photodiodes, mesa, field plate

PACS: 85.60.Dw, 85.60.Bt **DOI:** 10.1088/1674-1056/ab90f1

1. Introduction

AlGaN ultraviolet (UV) avalanche photodiodes (APDs) have attracted great attention and made tremendous progress due to their small sizes, low breakdown voltages, and wide energy bandgaps, which could make them a candidate in UV detection field to replace the photomultiplier tubes (PMTs). Up to date, the gain more than 10^4 for AlGaN UV APD has been successfully obtained.[1] However, in order to replace the PMTs (10^6) used in the UV region, the performances of AlGaN APD should be further improved. Recently, our works have been devoted to the research of hetero-structure separate absorption and multiplication (SAM) AlGaN APDs to improve the avalanche gain by inducing hole initial ionization and polarization effect.[2,3] Moreover, the edge termination structures, such as field plate, ion-implantation isolation, and bevel-mesa are often employed to improve the performances of APDs by suppressing the electric field at the edge or improving the uniformity of electric field distribution.[4,5] As is well known, the bevel angle should be very small in order to effectively suppress the early edge breakdown. Generally, the bevel angle is no more than 10°.[6,7] Nevertheless, small bevel angle will reduce significantly the active area of APDs, which can reduce the photo-generated current and weaken detection sensitivity.

In order to minimize the loss of the active area and meanwhile alleviate the electric field crowding, we propose two AlGaN APD termination structures. One is large-angle beveled mesa and field plate (FP) structure, and the other is triple-mesa and FP structure. It should be noted that the proposed termination structures can be realized through the current device process which is often used in fabricating avalanche photodiodes and field effect transistors.[8,9] The performances of the two SAM AlGaN APDs are carefully analyzed by Devedit and Altas software in Silvaco. The results show that the breakdown voltage and gain of the proposed APDs can be increased obviously compared with those of their counterparts without FP structure.

2. Structure, parameters and physical models

Figure 1(a) shows the schematic structure of the standard AlGaN SAM APD with bevel angle and FP termination structure. It consists of a 180-nm p-GaN layer ($N_a = 2\times10^{18}$ cm^{-3}), a 200-nm $Al_{0.1}Ga_{0.9}N$ multiplication layer ($N_d = 1\times10^{16}$ cm^{-3}), a 60-nm $Al_{0.1}Ga_{0.9}N$ charge layer ($N_d = 1\times10^{18}$ cm^{-3}), a 180-nm $Al_{0.1}Ga_{0.9}N$ absorption layer ($N_d = 1\times10^{16}$ cm^{-3}), and an 800-nm n-$Al_{0.2}Ga_{0.8}N$ layer ($N_d = 2\times10^{18}$ cm^{-3}) on the $Al_{0.3}Ga_{0.7}N$/AlN/sapphire template. Bevel angle Θ is 60°. The FP is placed on the top of the 500-nm Si_3N_4 passivation layer and extends to a multiplication layer along the sidewall. Figure 1(b) shows the schematic

*Project supported by the Natural Science Research Project of Anhui University, China (Grant No. KJ2019A0644), the National Natural Science Foundation of China (Grant Nos. 61634002 and 61804089), the Natural Science Alliance Foundation, China (Grant No. U1830109), the Natural Science Foundation of Anhui Province, China (Grant No. 1708085MF149), the Chuzhou University Research Project, China (Grant No. zrjz2019002), and the Project of the Higher Educational and Technology Program of Shandong Province, China (Grant No. J16LN04).

†Corresponding author. E-mail: djchen@nju.edu.cn

structure of the standard AlGaN SAM APD with triple-mesa and FP termination structure. The bottom mesa size is set to be 8.4 μm to keep the same width of absorption layer as that of the APD with bevelled mesa. The middle mesa and the top mesa size are set to be 6.4 μm and 5.2 μm respectively. The thickness and doping concentration of each layer are the same as those in Fig. 1(a). The thickness of Si_3N_4 is 180 nm. The n-$Al_{0.2}Ga_{0.8}N$ layer widths for both APDs are set to be 12 μm.

In simulation, the Poisson equation and carrier continuity equation are used. The carrier generation–recombination model includes SRH, Auger, surface, and optical recombination. The four dark currents for generation–recombination, drift–diffusion, trap-assistant tunneling, and band-to-band current are all taken into account. The photocurrent calculation is performed by two-dimensional (2D) ray trace and absorption model. As is well known, the dislocations and damage in AlGaN or GaN bulk can be translated into the bulk trap. Here, a single acceptor-type bulk trap density of 1×10^{12} cm^{-3} with capture cross section of trap of 1×10^{-15} cm^{-2} is used. The density of the surface trap is set to be 2×10^{12} cm^{-2}, and the recombination velocity for electrons and holes is 1×10^{7} cm/s. The impact ionization coefficient of AlGaN is fitted from our experiment values combined with those in Ref. [10]. The hole ionization coefficient for $Al_{0.1}Ga_{0.9}N$ in the present work is given by $a = 1.34 \times 10^{8}\,\mathrm{e}^{-1.7\times10^{7}/E}$, where E is the electric field, the absorption coefficient is calculated from the equation of $\alpha = 4\pi\kappa/\lambda$, in which k is the extinction coefficient. The other models and parameters are similar to those in our previous work.[11,12]

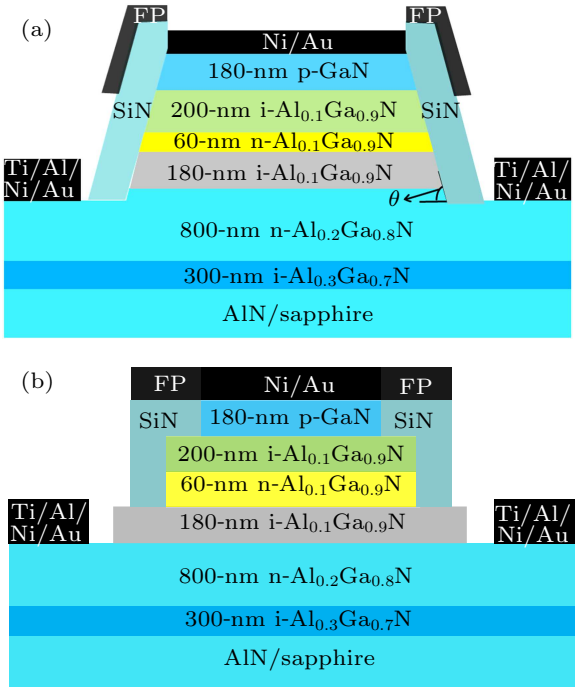

Fig. 1. Schematic structure of (a) standard AlGaN SAM APD with bevel angle and FP termination, and (b) standard AlGaN SAM APD with triple-mesa and FP termination.

3. Results and discussion

The dark current, photocurrent, and gain characteristics for the standard AlGaN APDs with FP and different bevel angles are calculated as shown in Fig. 2(a). Moreover, to better comprehend the influence of FP, the current–voltage (I–V) characteristics and gains for those corresponding AlGaN APDs without FP structure are presented in Fig. 2(c). The illuminated light wavelength is 340 nm and power density is 5×10^{-5} W/cm^2. As shown in Fig. 2(c), for APDs without FP structure, the breakdown voltage is 72.16 V and the avalanche gain is 5.5×10^4 when the bevel angle is 10° and the breakdown voltage significantly drops from 72.16 V for bevel angle 10° to 59.835 V 56.625 V, 57.727 V for bevel angles 20°,

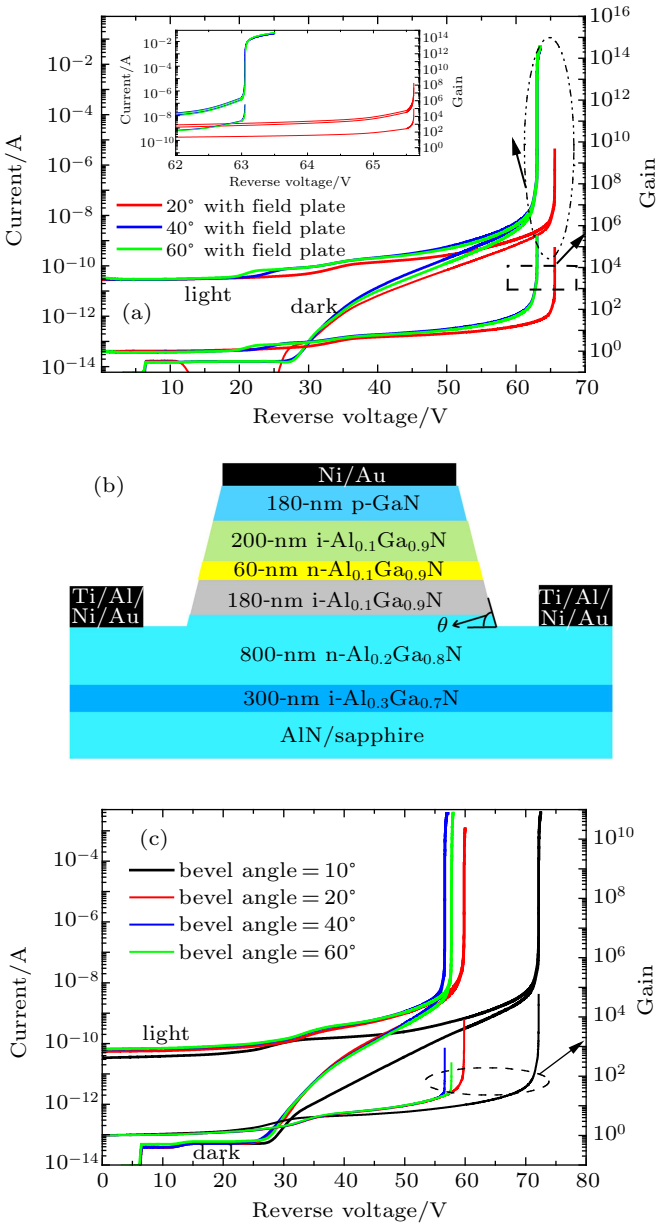

Fig. 2. (a) I–V characteristics in dark and under illumination and gain for AlGaN SAM APD with different bevel angles and FP structure, (b) schematic structure of AlGaN SAM APD without FP, and (c) I–V characteristics in dark and under illumination as well as gain for AlGaN SAM APD without FP.

40°, and 60° respectively. The gain decreases significantly to 7.71×10^3, 8.37×10^2, and 2.73×10^2 correspondingly. Here, the avalanche gain is calculated as done in Refs. [13,14] For three APDs with FP structure, the breakdown voltages are all over 63 V. The gain increases slightly from 8.28×10^4 to 3.05×10^5 as bevel angle increases. However, the gain of the APDs with FP structure is nearly two orders of magnitude higher than that without FP structure. From Figs. 2(a) and 2(c), we can see that the APD with 60° bevel angle has the highest photocurrent.

To analyze further the *I*–*V* characteristic and gain observed in Fig. 2, we firstly simulate the 2D electric field distributions for four APDs without FP structure at reverse bias 30 V, and the results are shown in Figs. 3(a)–3(d). In calculation, we choose the right half of the APD to improve the operation speed. It can be seen from Figs. 3(a)–3(d), showing that as bevel angle increases, the area of high electric field becomes larger in the multiplication layer. This can effectively enhance the cross sectional area of multiplication region and is in favour of the increase of photocurrent as observed in Fig. 2(c). Moreover, the maximum electric field moves from the bulk to the sidewall with bevel angle increasing, which may result in the electric field crowding and premature breakdown at the edge of APDs. To further analyze the electric field in multiplication layer, we calculate the electric field distribution along the x direction at $y = 190$ nm, $y = 280$ nm, and $y = 350$ nm, located at the upper, middle and lower of the multiplication layer, respectively, as presented in Figs. 3(e)–3(g). The $y = 0$ is defined as the position of upper surface of p-GaN. Figures 3(f) and 3(g) show that the distribution of electric field in bulk is very flat and is larger than at edge when y is 280 nm and 350 nm, respectively. It means that the early edge breakdown does not occur in the middle and lower section of the multiplication layer. The premature breakdown will mainly occur in the upper section of the multiplication layer as shown in Fig. 3(e). The maximum electric field is 1.68×10^6 V/cm, 1.72×10^6 V/cm, 1.91×10^6 V/cm, and 1.92×10^6 V/cm for the APDs with bevel angle of 10°, 20°, 40°, and 60°, respectively, when y is 190 nm. The maximum electric field arrives at the sidewall as the bevel angle exceeds 40°. As a result, the premature breakdown risk increases with bevel angle increasing.

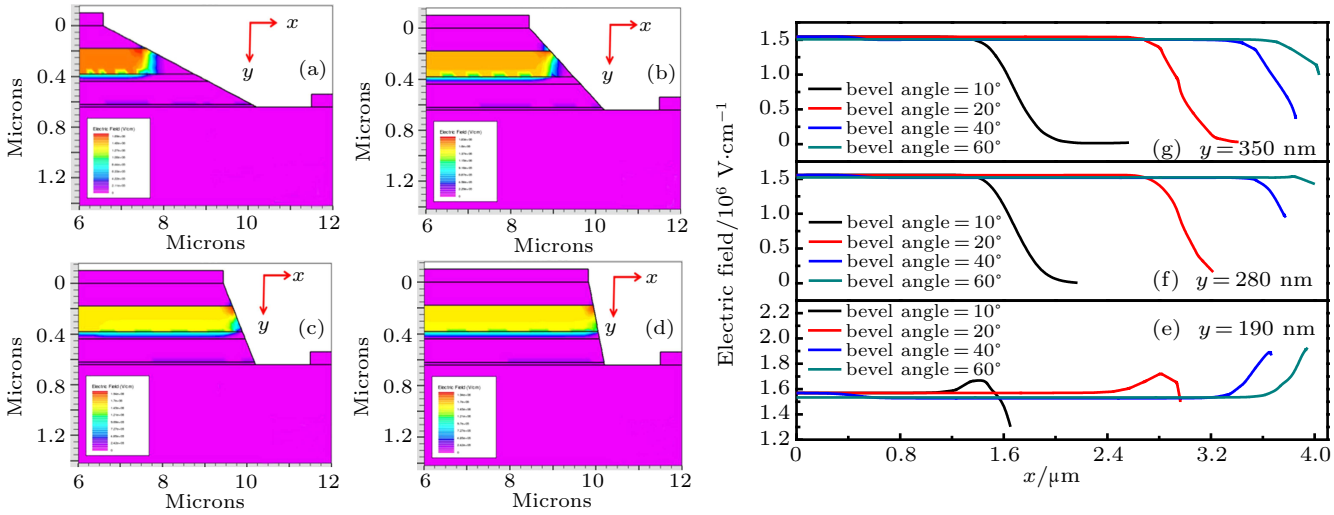

Fig. 3. Simulated two-dimensional electric field distribution for APD with bevel angle of (a) 10°, (b) 20°, (c) 40°, and (d) 60°, and electric field distribution along x direction in multiplication layer at (e) $y = 190$ nm, (f) $y = 280$ nm, (g) $y = 350$ nm with reverse bias 30 V.

As analyzed above, the premature breakdown tends to happen at the upper section of the multiplication layer for AlGaN APD with larger bevel angle. So, we design the PF structure only extending to the upper section of the multiplication layer as shown in Fig. 1(a). Next, we investigate the 2D electric field and electric field distribution along the x direction at $y = 190$ nm for the APD with 60° bevel angle and FP structure at a reverse bias of 30 V. As shown in Figs. 4(a) and 4(b), we find that the edge electric field significantly decreases for the APD with FP structure. It means that the designed FP structure can effectively suppress the electric field crowding at the edge and reduce the premature breakdown risk. Moreover, a higher electric field in an active region is allowed. Thus, a higher gain for the APD with large bevel angle and FP structure can be expected.

Another common method to suppress the edge electric field in AlGaN APD is to adopt double-mesa structure or triple-mesa structure.[1,15,16] In Fig. 1(b), we design a standard AlGaN APD with triple-mesa and FP structure. To analyze the influence of mesa size on performance of APD, we calculate the *I*–*V* curves and gains for the AlGaN APDs with FP and different sizes of the first mesa as illustrated in Fig. 5(a), where the size of the second mesa and the third mesa keep constant. In addition, to investigate the effect of FP, we also calculate

the *I–V* characteristic curves and gains as shown in Fig. 5(b) for the corresponding APD without FP structure (Fig. 5(c)) as a comparison. For the APD without FP, the breakdown voltages for sizes of the first-mesa 5.2 μm, 4 μm, and 1.6 μm are 64.174 V, 58.144 V, and 49.083 V, respectively, presenting a significantly declining trend with first-mesa size decreasing, and the gains are 6.45×10^3, 1.06×10^4, and 2.53×10^3, correspondingly. As for the APD with FP, the breakdown voltages are 75.628 V, 75.665 V, and 83.904 V for first-mesa sizes 5.2 μm, 4 μm, and 1.6 μm respectively. The gains are 1.9×10^5, 1.67×10^5, and 1.73×10^5, correspondingly, showing one order of magnitude higher than those of their counterparts without FP structure.

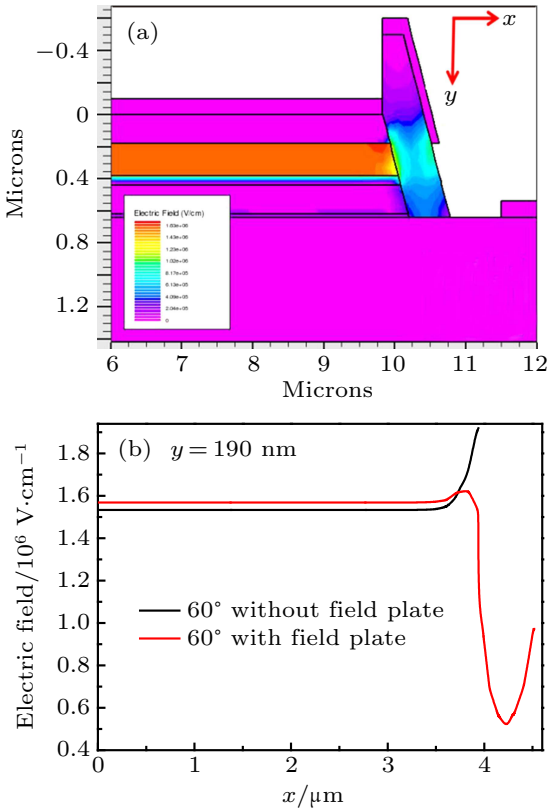

Fig. 4. (a) Two-dimensional electric field for AlGaN APD with 60° bevel angle and FP structure at reverse bias of 30 V, (b) electric field distribution along *x* direction in multiplication layer for 60° bevelled AlGaN APD with and without FP structure.

To illustrate the results in Fig. 5(b), the 2D electric field distributions for three triple-mesa APDs without FP are compared in Fig. 6 at the reverse bias of 30 V. The larger the first-mesa size, the wider the active multiplication region becomes, which results in a higher photocurrent as observed in Fig. 5(b). The low breakdown voltage for the AlGaN APD with small first-mesa size may be caused by the current crowding at the p-type GaN sidewall in the p–n junction depletion region because the maximum electric field is located there.

Figure 7 displays 2D electric field distributions at reverse bias of 30 V for the APD with FP structure and the first mesa size of (a) 5.2 μm, (b) 4 μm, and (c) 1.6 μm, respectively. The ideal APD structure without the first mesa or FP is also calculated in Fig. 7(d) as a comparison. In comparison with the APD without FP structure in Fig. 6, the electric field in the APD with FP extends to the sidewall from the bulk in the multiplication region, which can effectively increase the active area and improve the uniformity of electric field distribution. The strength is lower at the sidewall than in bulk, which is also unlike the scenario in an ideal structure. In addition, the FP can reduce the electric field strength at the sidewall of the p-type depletion region. Therefore, the APDs with FP can suppress electric field crowding at both sidewalls of upper p–n junction and increase the electric field strength in the active region, which is in favor of obtaining a higher gain.

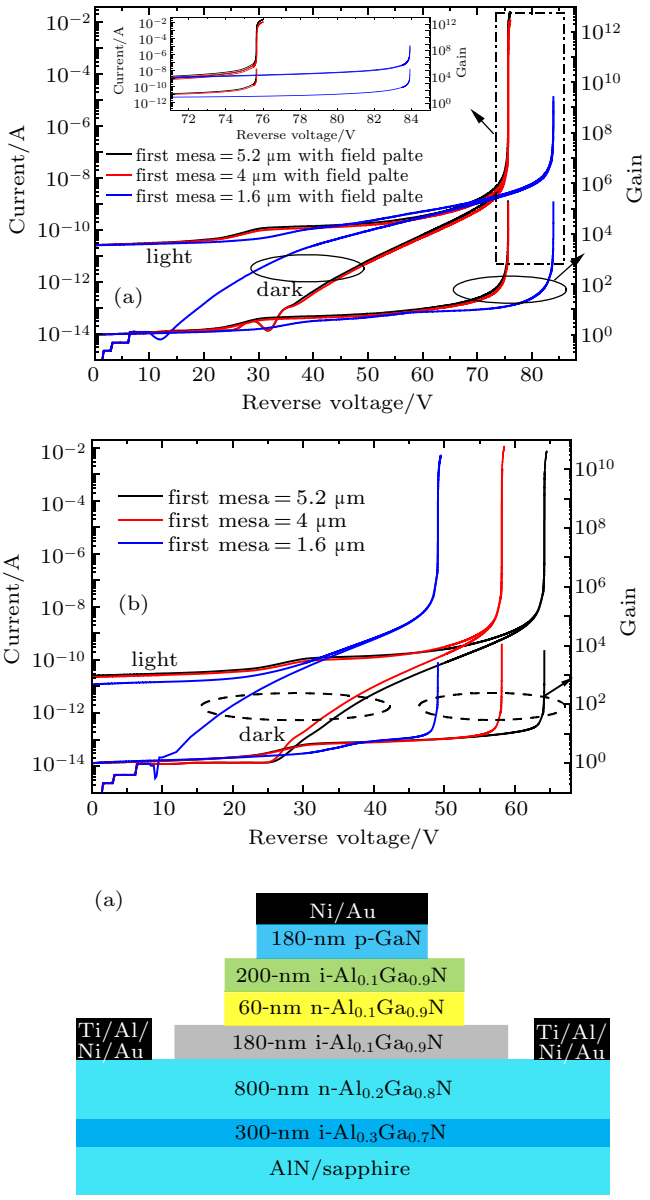

Fig. 5. *I–V* characteristic curves in dark and under illunination and gain for AlGaN APDs with different mesa sizes (a) with and (b) without FP. (c) Schematic structure of AlGaN APD with triple-mesa structure.

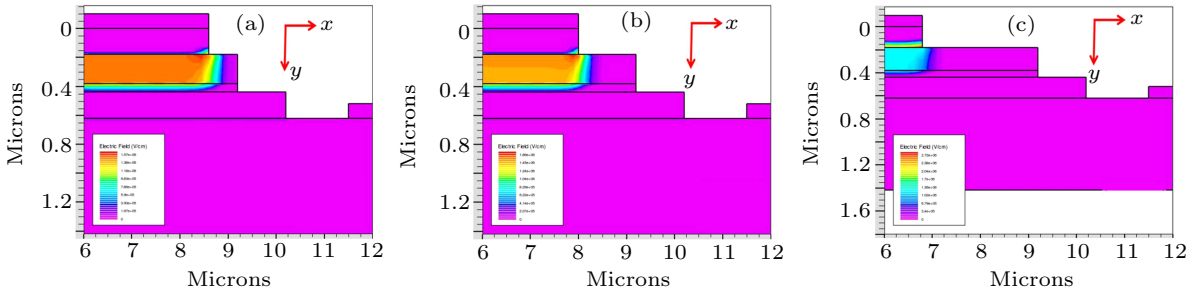

Fig. 6. Two-dimensional electric field distribution at reverse bias of 30 V for APD with first-mesa size (a) 5.2 μm, (b) 4 μm, and (c) 1.6 μm.

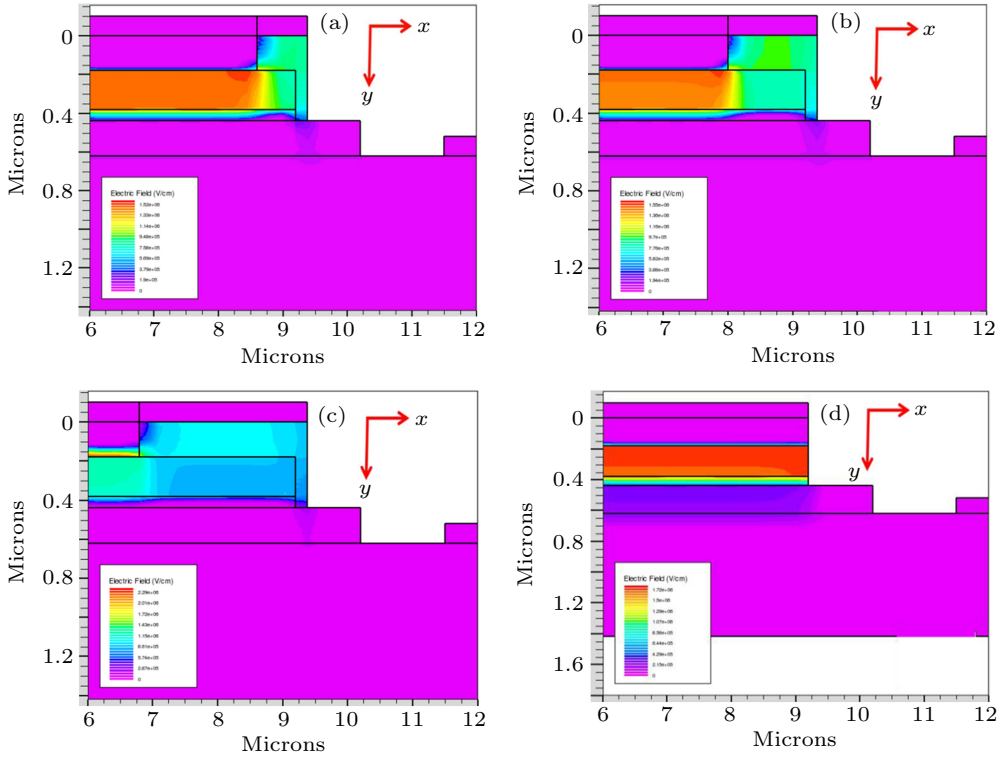

Fig. 7. Two-dimensional electric field distribution at reverse bias of 30 V for the APD with FP and first-mesa size (a) 5.2 μm, (b) 4 μm, (c) 1.6 μm, and (d) ideal structure.

4. Conclusions

In this work, the performances of the AlGaN SAM APDs combining the large bevel angle or triple-mesa with FP structure are investigated numerically. The results show that the APD with large bevel angle and FP structure can improve the detection sensitivity due to its larger active area, and can also significantly increase the gain compared with the corresponding APD without FP by suppressing edge electric field crowding. Meanwhile, the triple-mesa AlGaN APDs with FP structure have also a similar enhancement effect to the large-angle bevelled APDs, which is attributed to a smaller electric field strength at sidewall than in the bulk of multiplication layer.

References

[1] Cai Q, Luo W K, Li Q, Li M, Chen D J, Lu H, Zhang R and Zheng Y D 2018 *Appl. Phys. Lett.* **113** 123503
[2] Huang Y, Chen D J, Lu H, Dong K X, Zhang R, Zheng Y D, Li L and Li Z H 2012 *Appl. Phys. Lett.* **101** 253516
[3] Tang Y, Cai Q, Yang L H, Dong K X, Chen D J, Lu H, Zhang R and Zheng Y D 2017 *Chin. Phys. B* **26** 038503
[4] Kizilyalli I C, Prunty T and Aktas O 2015 *IEEE Electron Dev. Lett.* **36** 1073
[5] Reddy P, Breckenridge M H, Klump A, Guo Q, Mita S, Sarkar B, Kirste R, Moody B, Tweedie J, Collazo R and Sitar Z 2019 *IEEE Research and Applications of Photonics in Defense Conference (RAPID)* p. 1
[6] Pham T T T, Shin H, Chong E and Cha H Y 2018 *J. Semicond. Sci. Technol.* **18** 645
[7] Cha H Y 2010 *J. Korean Phys. Soc.* **56** 672
[8] Akiyama S, Kondo M, Wada L and Horio K 2019 *Jpn. J. Appl. Phys.* **58** 068003
[9] Mao W, Fan J S, Du M, Zhang J F, Zheng X F, Wang C, Ma X H, Zhang J C and Hao Y 2016 *Chin. Phys. B* **25** 127305
[10] Wang X D, Hu W D, Pan M, Hou L W, Xie W, Xu J T, Li X Y, Chen X S and Lu W 2014 *J. Appl. Phys.* **115** 013103
[11] Dong K X, Chen D J, Lu H, Liu B, Han P, Zhang R and Zheng Y D 2013 *IEEE Photon. Technol. Lett.* **25** 1510
[12] Liu Y L, Wang W, Dong Y, Chen D J, Zhang R and Zheng Y D 2019 *Acta Phys. Sin.* **68** 247203 (in Chinese)
[13] McClintock R, Yasan A, Minder K, Kung P and Razeghi M 2005 *Appl. Phys. Lett.* **87** 241123
[14] Sun L, Chen J, Li J and Jiang H 2010 *Appl. Phys. Lett.* **97** 191103
[15] Shao Z G, Chen D J, Lu H, Zhang R, Cao D P, Luo W J, Zheng Y D, Li L and Li Z H 2014 *IEEE Electron Dev. Lett.* **35** 372
[16] Liu H D, Zheng X G, Zhou Q G, *X G,* Mcintosh D C and Campbell J C 2009 *IEEE J. Quantum Elect.* **45** 1524